Satellite-based T-S Diagrams derived from SMOS, Aquarius and OSTIA data

Marlene Klockmann[1], Roberto Sabia[2], Diego Fernández-Prieto[3], Craig Donlon[4], Marco Talone[5] and Jordi Font[6]

[1]ESA, ESRIN, Frascati, Italy, Marlene.Klockmann@esa.int
[2]ESA, ESRIN, Frascati, Italy, Roberto.Sabia@esa.int
[3]ESA, ESRIN, Frascati, Italy, Diego.Fernandez@esa.int
[4]ESA, ESTEC, Noordwijk, the Netherlands, Craig.Donlon@esa.int
[5]SERCO SpA, Frascati, Italy, Marco.Talone@serco.com
[6]SMOS Barcelona Expert Centre, Barcelona, Spain, jfont@icm.csic.es

Abstract. Temperature Salinity (T-S) diagrams emphasize the relationship between observed values of temperature and salinity in the ocean and connect them to density. Specific T-S curves characterize water masses and can be used to identify them in regions other than their formation area. The SMOS and Aquarius/SAC-D satellite missions provide a means to study the temporal variation of the surface T-S signature for the first time on a global scale. The present study derives experimental satellite based T-S diagrams. The main objectives are to characterize the (co-) variability of Sea Surface Temperature (SST) and Sea Surface Salinity (SSS) and to understand the unique information that SMOS and Aquarius are providing with respect to existing climatology or in-situ data as well as the processes governing the distribution and variability of SSS. The T-S diagrams are produced from SMOS and Aquarius Optimal Interpolated SSS and OSTIA SST. They are compared with T-S diagrams derived from an ARGO Optimal Interpolated product and the World Ocean Atlas 2009 climatology, respectively. The temporal variability is studied for each ocean basin. Comparison with the ARGO based T-S diagrams might provide evidence of SSS biases and errors currently experienced by the satellites. A method is under investigation to separate the retrieval errors from the additional information that the satellite data may contain with respect to the ARGO data. Linking the information from the horizontal T-S diagrams with vertical profiles can hopefully provide insight into water mass formation and help to identify potential formation areas.

Keywords. Sea surface salinity, sea surface temperature, SMOS, Aquarius, OSTIA, water masses

1. Introduction

Temperature Salinity (T-S) diagrams emphasize the relationship between observations of ocean temperature and salinity and connect them to density. Typically they are derived from vertical profiles such as CTD casts. A specific T-S pair is called a water type, while a T-S curve (i.e. a range of values) is called a water mass. Water mass can also refer to a water body with the same formation history. A water mass is formed at the ocean surface under specific conditions which determine the temperature and salinity. Processes that modify water characteristics are precipitation (P) and evaporation (E), solar heating or surface cooling, freezing or melting of sea-ice, river run-off and horizontal/vertical advection and mixing. Assuming that T and S are conservative properties, i.e. that away from the surface they can only be modified by mixing, specific T-S curves can be used to identify water masses in regions other than their formation area and to trace their movements. On a global scale, water masses are typically divided into upper (0-500m), intermediate (500- 1500) and deep or bottom (>1500m) water masses. All of these water masses have their origins at the surface, where the bottom water with very cold temperatures is typically formed at high latitudes. An overview of the major water masses is given by [1]. An introduction to water mass formation can be

found in [2]. Until now, water mass classification has been dependent on in-situ measurements such as CTD casts which have poor temporal and spatial coverage. Typically the upper meters of the profiles are not taken into account, since measurements are less reliable there. With the SMOS [3] and Aquarius/SAC-D [4] missions, satellite observations of Sea Surface Salinity (SSS) have become available with global coverage and higher temporal frequency. Together with space borne Sea Surface Temperature (SST) measurements it is now possible for the first time to observe the surface T-S signature on a global scale and to assess also its temporal (co-)variability. Since water mass formation takes place during the winter months, when deep convection is possible and no seasonal thermocline prevents the surface water from penetrating into greater depths, especially the winter surface T-S signature can provide a link to the evolution of water masses in deeper layers. This study presents experimental satellite-based, horizontal T-S diagrams as a means to study the temporal evolution of covariability of SST and SSS. The main objectives are to characterize the variability of SSS in relation to existing climatology, to understand the unique information that SMOS and Aquarius SSS data are providing with respect to climatology or in-situ measurements and to improve our understanding of the processes governing the distribution and variability of SSS. In the present study, T-S diagrams are produced from SMOS and Aquarius Optimal Interpolated (OI) SSS (Level 3 products, L3) and the Operational Sea Surface Temperature and Sea Ice Analysis (OSTIA) SST [5]. The satellite-based T-S diagrams are compared with ARGO based T-S diagrams which use SST and SSS from Near Real Time ARIVO monthly fields (in the following referred to as ARGO NRT) [6]. Comparison with the these T-S diagrams might provide evidence of SSS biases and errors currently experienced by the satellites (due to e.g. the roughness models applied in the SSS retrieval at L-band or external noise sources such as Galactic noise, Sun glint or RFI, [7]). SST and SSS from the World Ocean Atlas 2009 (WOA 09, [8,9]) are used for the comparison with climatology. Section 2 gives a short overview of the data sets used in this study and of methods applied. Section 3 presents first results and section 4 provides a brief discussion and outlines future work.

2. Methods

2.1. Data sets

ESA's SMOS mission was launched in November 2009 and is in its operational phase since May 2010. Its Microwave Imaging Radiometer using Aperture Synthesis (MIRAS) measures brightness temperature at L-Band from multiple incidence angles. Sea Surface Salinity (SSS) is then retrieved with an iterative inversion scheme [10]. We use a monthly SMOS L3 OI product with a spatial resolution of 1˚ by 1˚ derived from ascending passes obtained with v550 of the L2OS processor. Aquarius/SAC-D is a combined active/passive US/Argentinean mission launched in June 2011 and it is operational since December 2011. A key capability of Aquarius lies in its L-band scatterometer which provides collocated roughness information needed as auxiliary parameter for a proper SSS retrieval [11]. We use Aquarius v2.0 L3 SSS smoothed monthly fields with a spatial resolution of 1˚ by 1˚ [12]. The OSTIA data set provides daily foundation temperature fields derived from the satellites of the Group of High Resolution SST (GHRSST) project, merged with in-situ observations and optimally interpolated to a grid with 1/20˚ resolution [5]. We have averaged the daily fields to a monthly product with a 1˚ by 1˚ resolution. For the ARGO NRT fields the Near Real Time ARGO profiles provided by Coriolis are quality checked and interpolated onto a regular grid in combination with other local arrays (mooring and CTD data) using the In Situ Analysis System (ISAS, [13]). Monthly fields are provided with a 0.25˚ by 0.25˚ resolution at the equator. The latitudinal resolution increases towards the poles. We have averaged the fields to a 1˚ by 1˚ grid. The WOA 09 data set provides a climatology of ocean temperature and salinity on a 1˚ by 1˚ grid composed of the objectively analysed in-situ data available in the World Ocean Database from 1955

to 2006. The time period of the study is currently limited to 2011, since the ARGO NRT product has only recently been reprocessed and updated to 2012. Therefore we are using the entire year of 2011 of SMOS and five months (August to December 2011) of Aquarius data.

2.2. *Horizontal T-S diagrams and temporal variability*

Based on the water mass classification of [1], we have divided the global ocean into seven major ocean basins (Figure 1). For each region SST is plotted against SSS. This has been done for monthly and seasonally averaged data. Density is calculated using the equation of state TEOS10 [14]. Therefore temperature and salinity have been converted to conservative temperature (given in ˚C) and absolute salinity (given in g/kg). Otherwise salinity will be given in psu (practical salinity unit) according to the Practical Salinity Scale (PSS78). For the comparisons with ARGO NRT and WOA 09 we have also calculated the differences between OSTIA SST and ARGO NRT/WOA 09 SST and between SMOS/Aquarius SSS and ARGO NRT/WOA 09 SSS respectively and plot dSST against dSSS. In order to better understand seasonal variability of the SSS pattern, we have also calculated the seasonal cycle as a spatial average within each region for every month.
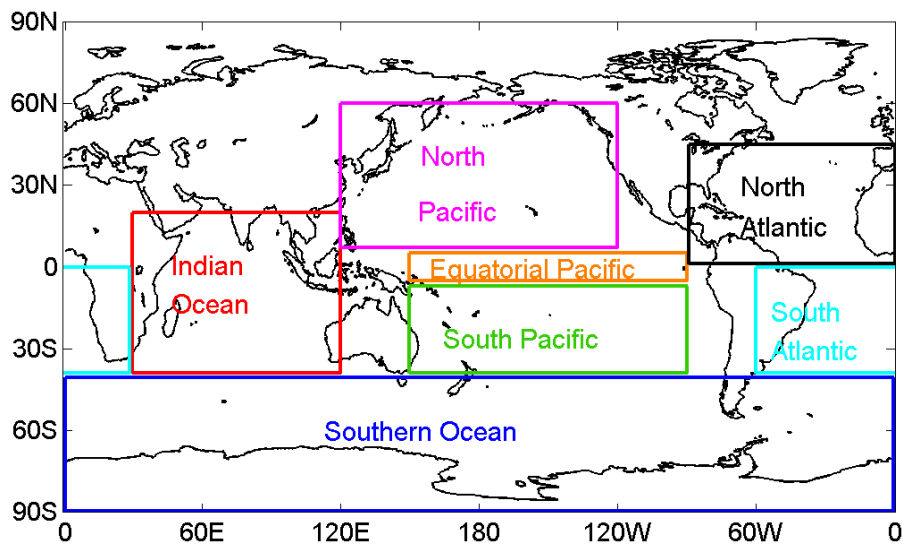

Figure 1. Map showing the selected seven areas

2.3. *Potential formation areas*

A first attempt to connect the TS diagrams to the observation of water masses has been to trace the characteristic SST and SSS ranges of the major water masses specified in [1], i.e. in which months and in which areas the horizontal T-S signature is in agreement with the vertical profile of a specific water mass. The extension of these areas is compared for the different products and also compared with the 'best guess' formation areas indicated in [1].

3. Results

3.1. *T-S diagrams and dSST vs. dSSS*

Figures 2 and 3 show the seasonally averaged T-S diagrams and the corresponding dSST vs. dSSS plots for the North Pacific and the South Atlantic (other areas not shown). The North Pacific displays a large range of SST since the region contains both subpolar and subtropical waters. Water

211

with colder SST tends to have also fresher SSS. The SSS range is relatively constant over the four seasons, while the SST range in summer (JAS) is about 7K smaller with respect to the other seasons.
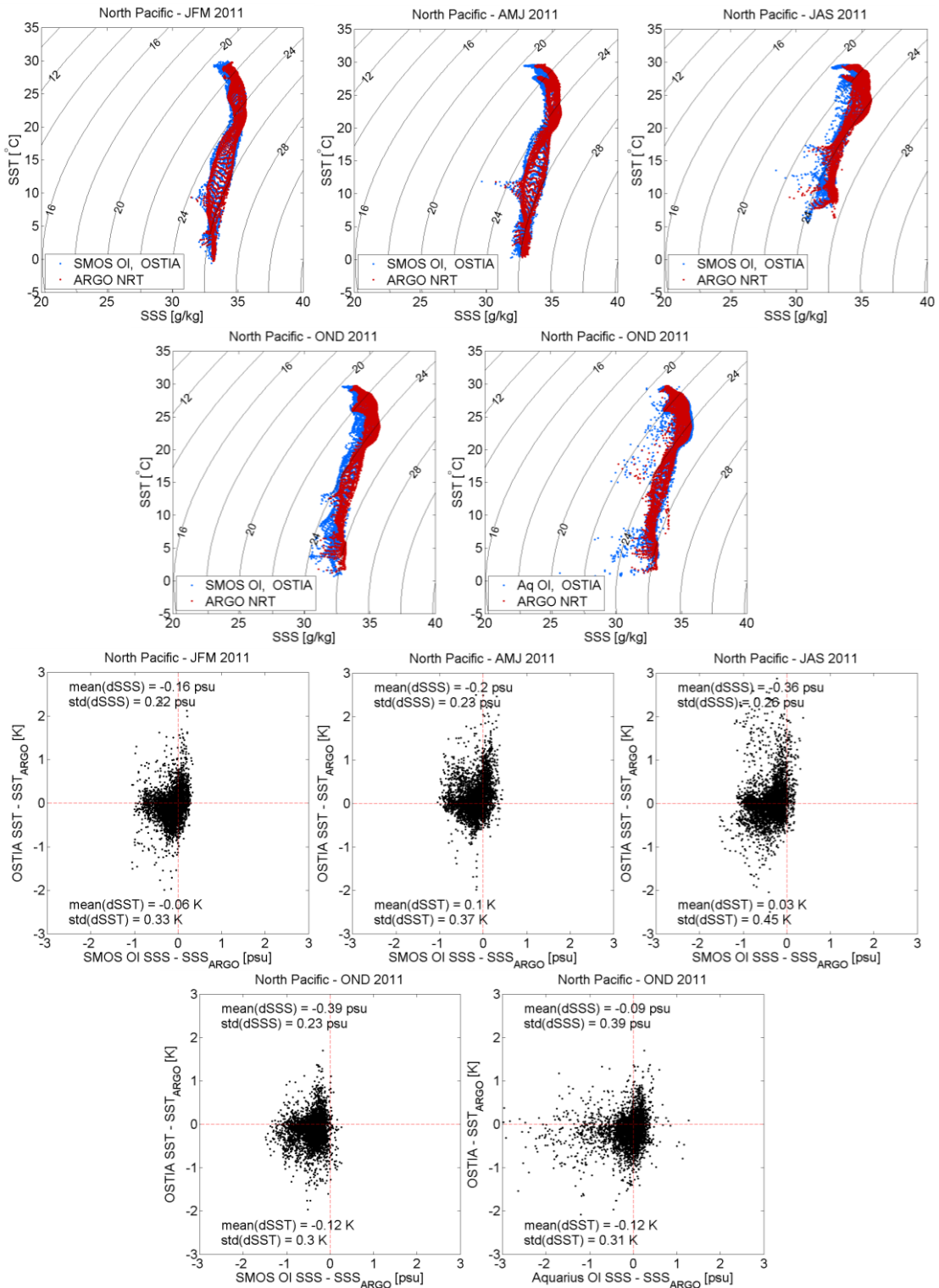

Figure 2. (upper panels) Seasonal averages of T-S diagrams for the North Pacific. Contour lines indicate surface density σ [kg/m³ -1000 kg/m³]. (lower panels) Seasonal averages of dSST vs dSSS calculated with respect to the ARGO NRT data. The spatial mean and standard deviation of dSSS and dSST are noted on the respective plots.

An interesting feature is the rib-like pattern which occurs during boreal winter and spring for SST between 5°C and 17°C and is seen by all three data sets (WOA 09 not shown). SMOS and Aquarius show very similar patterns compared with ARGO NRT but SMOS is on average 0.39 psu fresher in the second half of the year (JAS and OND) while Aquarius is almost unbiased (mean(dSSS)) = - 0.09 psu). The spatial standard deviation of dSSS lies between 0.22 and 0.26 psu for SMOS and is 0.39 psu for Aquarius.
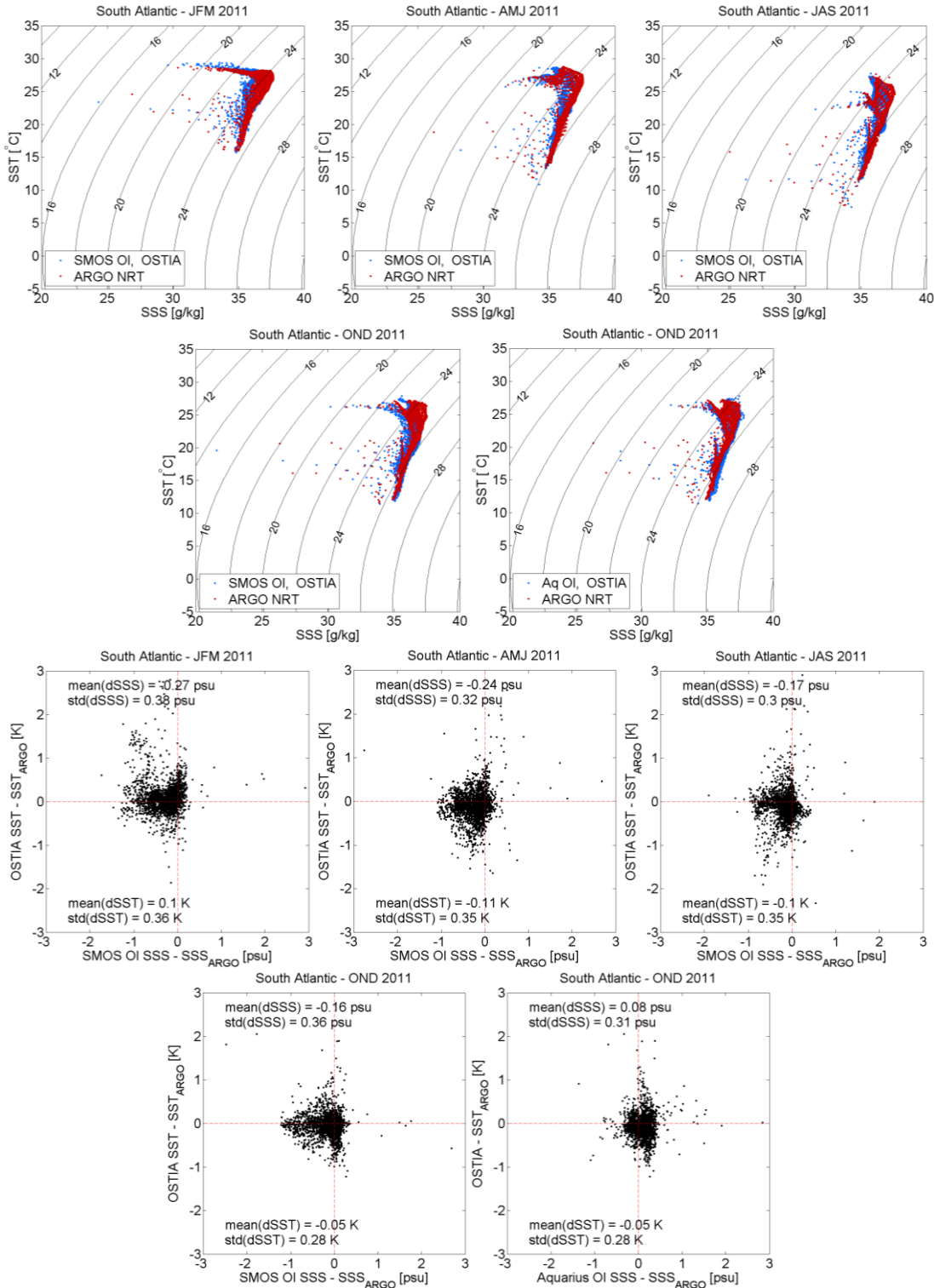

Figure 3. As Figure 2 for the South Atlantic

In the South Atlantic the SST range is smaller with 12-28°C. Also here colder SST are connected with fresher SSS. Only for SSTs above 25°C also SSS as low as 31-32 g/kg can be observed. This is seen in all three data sets (WOA 09 again not shown), especially during austral summer (JFM). SMOS shows again fresher SSS with a bias of -0.27 and -0.24 psu in JFM and AMJ, respectively. For the second half of the year the bias is reduced to -0.16 psu. The spatial standard deviation for SMOS SSS lies between 0.3 to 0.38 psu and is 0.31 psu for Aquarius.

3.2. Seasonal variability of SSS

Figure 4 shows the spatial mean SSS and standard deviation for every month for the North Pacific and the South Atlantic. In the North Pacific ARGO NRT (red curve) and WOA 09 (orange) show a small seasonal cycle with a peak-to-peak amplitude of 0.3 psu and 0.23 psu, respectively. SMOS (blue) is considerably fresher than ARGO NRT, WOA 09 or Aquarius except for April 2011. The standard deviation however is comparable. Aquarius (green) is in good agreement with ARGO NRT but shows a larger standard deviation, especially in November and December.

The South Atlantic displays an almost constant average SSS of about 36 psu (ARGO NRT and WOA 09). ARGO NRT shows the largest standard deviation. The difference between ARGO NRT/WOA 09 and SMOS is largest from January to May and decreases towards the end of the year. Aquarius shows slightly saltier SSS as compared to ARGO NRT or WOA 09.
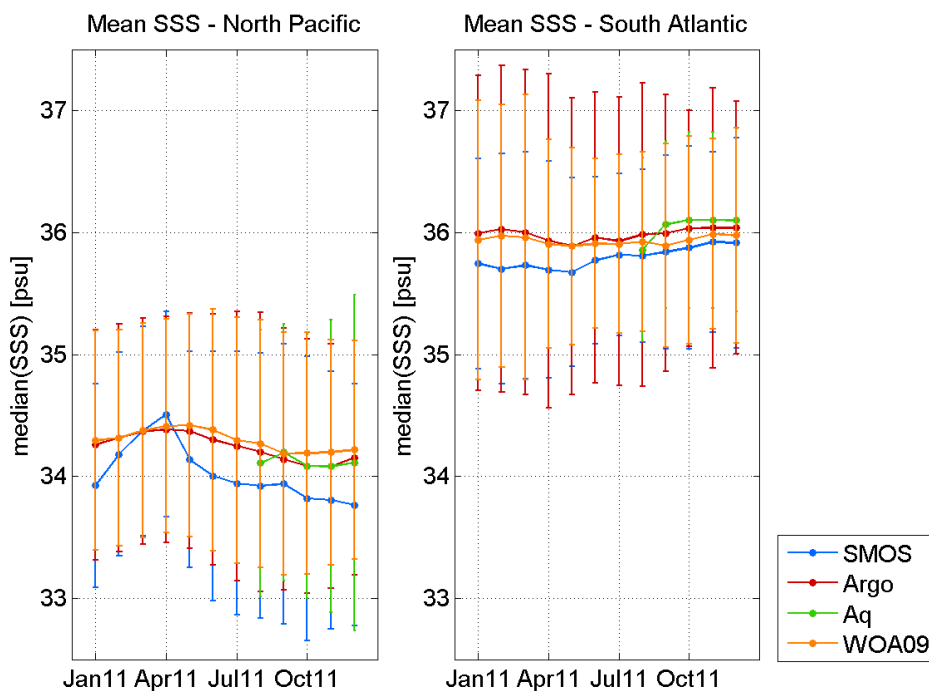

Figure 4. Seasonal cycle of spatially averaged SSS for the North Pacific (left) and the South Atlantic (right). The respective products are colour-coded. Error bars indicate the standard deviation.

3.3. Potential formation areas

Figure 5 shows potential formation areas for the Western North Pacific Central Water (WNPCW) and Eastern North Pacific Central Water (ENPCW). The T-S ranges of these two water masses are quite similar with 10-22°C/34.2-35.2 psu and 12-20°C/34.2-35 psu for WNPCW and ENPCW, respectively. Therefore we have combined them for a first attempt to define potential formation areas. As mentioned before, water mass formation takes place during the winter months.

214

In these months the horizontal surface T-S signature should be very similar to a vertical T-S profile. As can be seen from Figure 2 especially the SST range is much larger than the specified 10-22 ˚C. In areas with warmer SST, stratification may play an important role in preventing water mass formation. Areas with colder SST could be potential formation areas for other water masses.
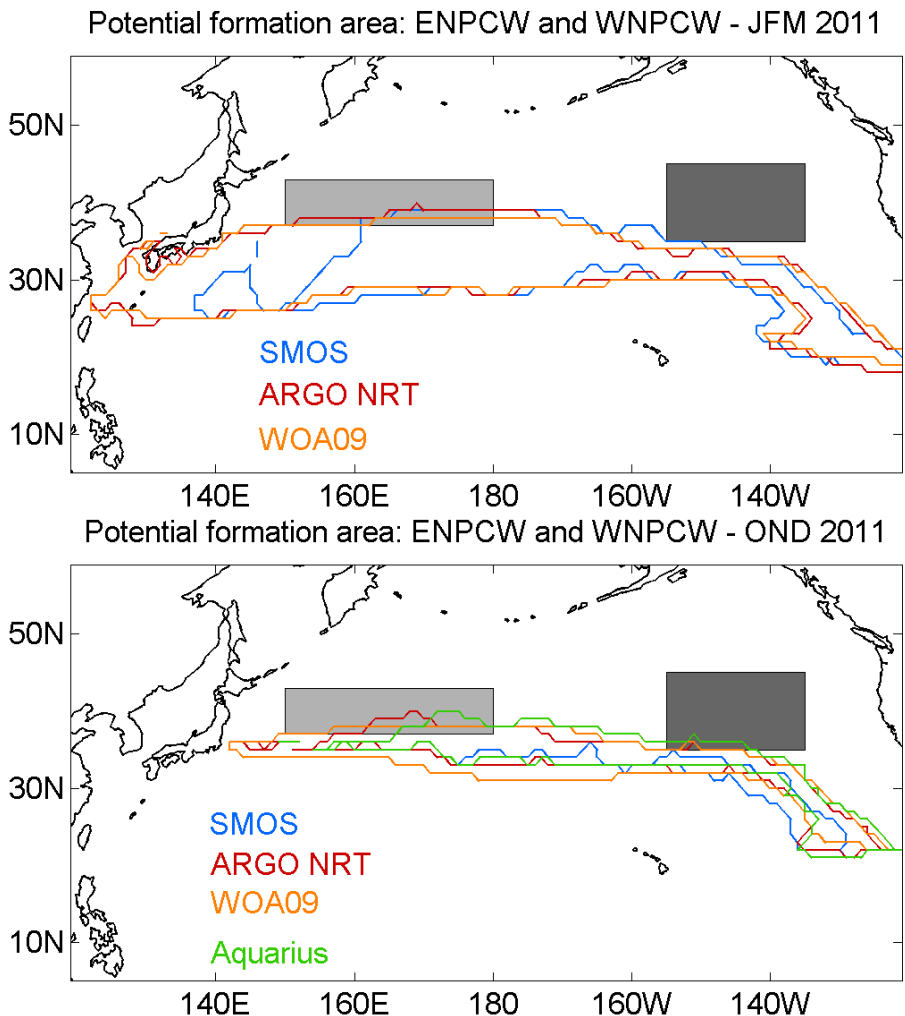

Figure 5. Potential formation areas for the water masses Eastern North Pacific Central Water (dark grey) and Western North Pacific Central Water (light grey) according to [1]. The upper (lower) panel shows the areas where the winter (autumn) average of SST and SSS are within the ranges 10-22˚C and 34.2-35.2 psu, respectively. Each contour represents the border of the spatial extent for the respective products.

During winter (JFM) SMOS/OSTIA, ARGO NRT and WOA 09 show a very similar geographical distribution. The area covered by SMOS is somewhat smaller in the west, probably due to quality control data flagging near the coast line. The formation areas indicated by [1] are located further north and cover a much smaller area. The latter may be due to the fact that a water mass is not only defined by its range of values but also by a specific relation in the vertical. For WNPCW the indicated formation area (light grey box) has some overlap with the geographical distribution indicated by the contour lines. For the ENPCW (dark grey box) there is no overlap in winter and a very small overlap in autumn.

During autumn (OND) the extension of the potential formation areas is smaller, especially on the western side. This can be expected as the surface cooling is just beginning in autumn, i.e. SSTs are not yet cold enough and stratification may still play a larger role. Aquarius is in good agreement

with ARGO NRT, the area inferred from SMOS is again smaller as compared to either of the three products.

Further studies are necessary to understand the surface signature of water masses and the link between the horizontal and vertical T-S relationships.

4. Conclusions

The availability of SMOS and Aquarius data makes it possible for the first time to study the temporal variability of the surface T-S signature. Therefore it is crucial to understand the nature of the differences (in the following referred to as mismatches) between the satellite data and climatology or in-situ data. Some part of the mismatches will be caused by retrieval errors but others could be induced by geophysical signals, such as near surface stratification during rain events [15],which is not detectable in the ARGO NRT data. We are currently investigating methods to separate the SSS retrieval errors from the additional information that the satellite data may contain with respect to the ARGO NRT or WOA 09 data. Therefore we have classified the T-S mismatch (Figures 2 and 3, bottom panels) into four categories (quadrants in Figure 6, left panel). The right panel of Figure 6 shows the geographical mismatch distribution in combination with contours of E-P. In this case, areas in which precipitation exceeds evaporation coincide well with areas in which SMOS sees fresher SSS than ARGO NRT (cyan and yellow quadrants). There are however also areas in which such collocations cannot be found. Further studies are needed in order to understand the full information provided by the T-S mismatch. We are planning to assess also the impact of other factors, e.g. wind speed or RFI, on the mismatches.
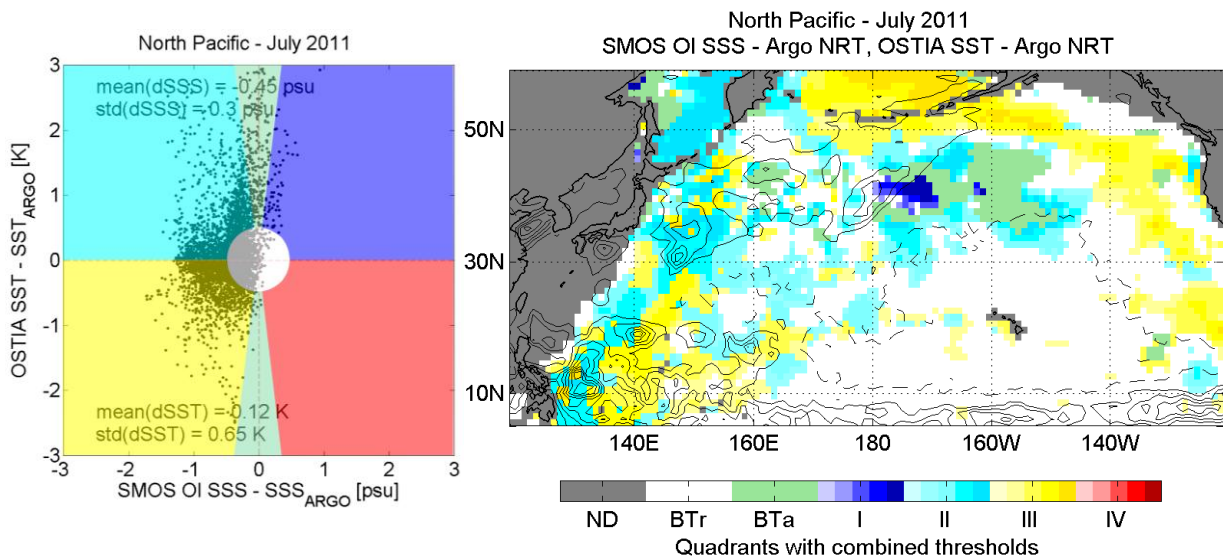

Figure 6. An example of combined mismatch (right) with contours of E-P superimposed (solid contours: P>E, dashed contours: E>P), contour levels are 3 mm/day, the zero contour line has been omitted. We use precipitation from CMORPH [16] and evaporation from OAFlux [17]. The colour scheme is explained on the left according to the dSST vs dSSS plot in Figures 2 and 3 (e.g. cyan: overestimation of SST, underestimation of SSS). The more intense the colour, the larger the mismatch. A mismatch smaller than 0.5 is indicated in white, mismatches which are mostly SST driven are indicated in light green.

Future work will also include additional datasets. We are planning to use L3 binned products of both SMOS and Aquarius. The SMOS Barcelona Expert Center has recently released a reprocessed SMOS product at 0.25˚ resolution which aligns the 2012 data set with the last reprocessing campaign. This data and the updated ARGO NRT data make it possible to extend the study period to

2012, so that we will have two complete years of SMOS data and almost one year and a half of Aquarius data. Further we intend to refine the geographical study areas (e.g. using SST gradients as boundaries or focusing only on potential formation areas). Longer time series will help to better understand the seasonal signal and in the long term to identify shifts or trends in the surface water mass formation.

Acknowledgements

References

[1] Emery, W. J., 2003. *Ocean Circulation / Water Types and Water Masses*. (Elsevier science) 1556-1567

[2] Tomzcak, M. & Godfrey, J. S., 2001. *Regional Oceanography: An Introduction* (online pdf version) 391 pp.

[3] Font, J., Camps, A., Borges, A., Martín-Neira, M., Boutin, J., Reul, N., Kerr, Y. H., Hahne, A., & Mecklenburg, S., 2010. *SMOS: The challenging sea surface salinity measurement from space*. Proceedings of the IEEE 98, 649-665

[4] Lagerloef, G., Colomb, R., Le Vine, D., Wentz, F., Yueh, S., Ruf, C., Lilly, J., Gunn, J., Chao, Y., deCharon, A., & Swift, C., 2008. *The Aquarius/SAC-D mission - Designed to meet the salinity remote sensing challenge*, Oceanography 21(1), 68–81

[5] Donlon, C. J., Martin, M., Stark, J. D., Roberts-Jones, J., Fiedler, E., & Wimmer, W., 2011. *The Operational Sea Surface Temperature and Sea Ice analysis (OSTIA)*. Remote Sensing of the Environment 116, 140-158

[6] Gaillard, F., Autret, E., Thierry, V., Galaup, P., Coatanoan, C., and Loubrieu. T., 2009. *Quality control of large ARGO data sets*. Journal of Atmospheric and Oceanic Technology 26(2), 337–351

[7] Font, J., Boutin, J., Reul, N., Spurgeon, P., Ballabrera-Poy, J., Chuprin, A., Gabarró, C., Gourrion, J., Guimbard, S., Hénocq, C., Lavender, S., Martin, N., Martínez, J., Mcculloch, M., Meirold-Mautner, I., Mugerin, C., Petitcolin, F., Portabella, M., Sabia, R., Talone, M., Tenerelli, J., Turiel, A., Vergely J.-L., Waldteufel, P., Yin, X., Zine, S., Delwart, S., 2012. *SMOS first data analysis for sea surface salinity determination*. International Journal of Remote Sensing 34(9-10), 3654–3670

[8] Locarnini, R. A., Mishonov, A. V., Antonov, J. I., Boyer, T. P., Garcia, H. E., Baranova, O. K., Zweng, M. M., and Johnson, D. R., 2010. *World Ocean Atlas 2009, Volume 1: Temperature.* S. Levitus, Ed. NOAA Atlas NESDIS 68, (U.S. Government Printing Office, Washington, D.C.), 184 pp.

[9] Antonov, J. I., Seidov, D., Boyer, T. P., Locarnini, R. A., Mishonov, A. V., Garcia, H. E., Baranova, O. K., Zweng, M. M., and Johnson, D. R., 2010. *World Ocean Atlas 2009, Volume 2: Salinity.* S. Levitus, Ed. NOAA Atlas NESDIS 69, (U.S. Government Printing Office, Washington, D.C.), 184 pp.

[10] Zine, S., Boutin, J., Font, J., Reul, N., Waldteufel, P., Gabarró, C., Tenerelli, J., Petitcolin, F., Vergely, J. L., Talone, M., and Delwart, S., 2008. *Overview of the SMOS Sea Surface Salinity Prototype Processor.* IEEE Transactions Geoscience and Remote Sensing 46(3), 621-645

[11] Le Vine, D. M., Lagerloef, G. S. E., Torrusio, S. E., 2010. *Aquarius and Remote Sensing of Sea Surface Salinity from Space*, Proceedings of the IEEE 98(5), 688-703

[12] Lilly, J. M. & Lagerloef, G. S. E. 2008. *Aquarius Level 3 processing algorithm theoretical basis document: Version 0.9.* (Aquarius Ground Segment, Goddard Space Flight Center) 14 pp.

[13] Gaillard, F., 2012. *ISAS-Tool Version 6: Method and Configuration, SO-ARGO report,* 45 pp.

[14] McDougall, T. J. & Barker P. M. , 2011. *Getting started with TEOS-10 and the Gibbs Seawater (GSW) Oceanographic Toolbox*, (SCOR/IAPSO WG127), 28 pp.

[15] Boutin, J., Martin, N., Reverdin, G., Yin, X., Gaillard, F., 2013. *Sea surface freshening inferred from SMOS and ARGO salinity: impact of rain*. Ocean Science 9, 183-192

[16] Joyce, R. J., Janowiak, J. E., Arkin P. A., & Xie, P., 2004. *CMORPH: A method that Produces Global Precipitation Estimates from Passice Microwave and Infrared Data at High Spatial and Temporal Resolution.* Journal of Hydrometeorology 5, 487-503

[17] Yu, L., Jin, X. & Weller, R. A., 2008. *Multidecade Global Flux Datasets from the Objectively Analyzed Air-sea Fluxes (OAFlux) Project: Latent and Sensible Heat Fluxes, Ocean Evaporation, and Related Surface Me-*

teorological Variables. Woods Hole Oceanographic Institution OAFlux Technical Report (OA-2008-01), 64 pp.